Validation of correlations-based transition modeling strategies applied to the Spalart-Allmaras turbulence model for the computation of separation-induced transition

Michel Bouchard, Julien Marty, Sebastien Deck, Michel Costes

Validation of correlations-based transition modeling strategies applied to the Spalart-Allmaras turbulence model for the computation of separation-induced transition

Bouchard M.[a,*], Marty, J.[b], Deck, S.[c], Costes, M.[d]

8 rue des Vertugadins, Meudon, FRANCE

[a] *Phd student ; Aerodynamics, Aeroelasticity and Acoustics Department ; Helicopters, Propellers and Turbomachinery Unit (H2T)*
[b] *Research Scientist ; Aerodynamics, Aeroelasticity and Acoustics Department ; Helicopters, Propellers and Turbomachinery Unit (H2T)*
[c] *Research Scientist ; Aerodynamics, Aeroelasticity and Acoustics Department ; Advanced Turbulence Modeling and Simulation Unit (MSAT)*
[d] *Research Scientist ; Aerodynamics, Aeroelasticity and Acoustics Department ; Advanced Turbulence Modeling and Simulation Unit (MSAT)*

Abstract

Predicting the laminar-turbulent transition is becoming a necessity in order to reduce margin costs in the design of turbines and helicopter rotors. Most RANS models lack the capacity to create turbulence sufficiently abruptly to accurately predict separation-induced transition. This paper aims at evaluating the performances of the $\gamma - Re_{\theta,\mathrm{t}}$ strategy applied to the models by Spalart-Allmaras and $k-\omega-$SST models ($\tilde{\nu} - \gamma - Re_{\theta,\mathrm{t}}$ and $k - \omega - \gamma - Re_{\theta,\mathrm{t}}$). The chosen test case features a laminar separation bubble over a flat plate. The results are compared to the flows obtained using classical algebraic criteria and validated against DNS data. The effects of the correction by Dacles-Mariani et al. are detailed as well as those of two sets of correlations.

The turbulence production mechanism of the present models is too weak downstream of the first increase of intermittency, and the laminar separation bubbles are longer than in the reference flow. More specifically, the $\tilde{\nu} - \gamma - Re_{\theta,\mathrm{t}}$

*Corresponding author
Email address: michel.bouchard@onera.fr (Bouchard M.)

model with Medida and Baeder's correlations fails to reach the correct levels of turbulence production in the fully turbulent boundary layer. Switching the correlations corrects this last behavior. Finally, using maps of the activation zones of the Dacles-Mariani correction, a sensor is exhibited that could be used in future separation-induced transition modeling efforts.
Keywords: Langtry-Menter, laminar, turbulent, transition, separation, reattachment, boundary layer, RANS, modelling

---

1. Introduction

Laminar or transitional boundary-layer separation has been shown to play a determining role in the performance of numerous aircraft systems, and more specifically of turbomachinery - both turbines and compressors [1, 2] - and helicopter rotors [3]. In these cases, a massive separation of the laminar boundary layer can lead to a complete stall of the airfoil, thereby drastically modifying the flow dynamics and pressure distribution along the surface. In turn, these changes in the topology of the flow affect the lift and drag of the airfoil. However, for closed separation bubbles, the reattachment location strongly depends on the laminar-turbulent transition phenomena that can be triggered by separation : if transition occurs, reattachment can significantly move upstream, decreasing the losses as compared to a fully laminar flow. Therefore, being able to understand and accurately predict separation-induced transition allows for a reduction of margins and a more efficient design.

A large number of studies have been conducted to understand the underlying principles of separation-induced transition [4–6]. A classification method for different types of separations, and, more importantly, different dynamics was introduced by Hatman and Wang (1998) [7]. These authors studied flows subjected to deceleration or adverse pressure gradient in which laminar separation is likely to occur. Their classification splits the cases between separations of locally stable laminar flow and of flows which are already subject to some destabilizing effect, such as Tollmien-Schlichting instabilities. They denote the latter case as

a "transitional separation". In both cases, the dominant destabilizing effect is a Kelvin-Helmholtz inviscid inflectional instability of the separated shear layer created by the recirculating fluid of the bubble. However, the initial perturbations of the shear layer are not of the same order of magnitude, since they have already been amplified in the transitional separation case. In both cases, studies have reported the advent of an abrupt transition involving a strong production of turbulence [8–11], though its properties (spectrum, coherent structures) differ from those of a wall-bounded turbulent flow until several bubble lengths downstream of reattachment [8]. Furthermore, Hatman and Wang distinguish "short" laminar separation bubbles from "long" ones according to the position of the mid-transition station (where $\overline{u'^2}$ reaches its maximum) relative to the reattachment location : in the case of a short bubble, the maximum of $\overline{u'^2}$ is reached roughly at the reattachment point, while in the long bubble case, reattachment occurs downstream of the mid-transition point. There is no consensus in the literature regarding these definitions [8, 12]. The classification by Hatman and Wang is used here.

This paper's main focus is a short laminar separation bubble [7]. Figure 1 presents a schematics of a typical short separation bubble. The bubble is comprised of a single recirculation region through which transition begins. According to Dick and Kubacki (2017) [13], the transition does not need to be complete for reattachment to occur. Still, the pressure recovery due to the production of turbulence is a strong contributing factor to the reattachment process. The recirculating region can be roughly described as including an upstream dead-air zone and a downstream vortex which can detach and be advected downstream. Therefore, the topology of a laminar separation bubble is highly unsteady. For instance, Roberts and Yaras (2005) [9] report a low frequency oscillation of the bubble length with an amplitude of 30 % of its average length. As shown on figure 1, the displacement thickness of the boundary layer reaches a maximum, then decreases, while the momentum thickness strongly increases in the aft part of the bubble. Downstream of the reattachment location, both thicknesses recover to a fully-turbulent behavior.

Figure 1: Typical flow topology downstream of a laminar separation.

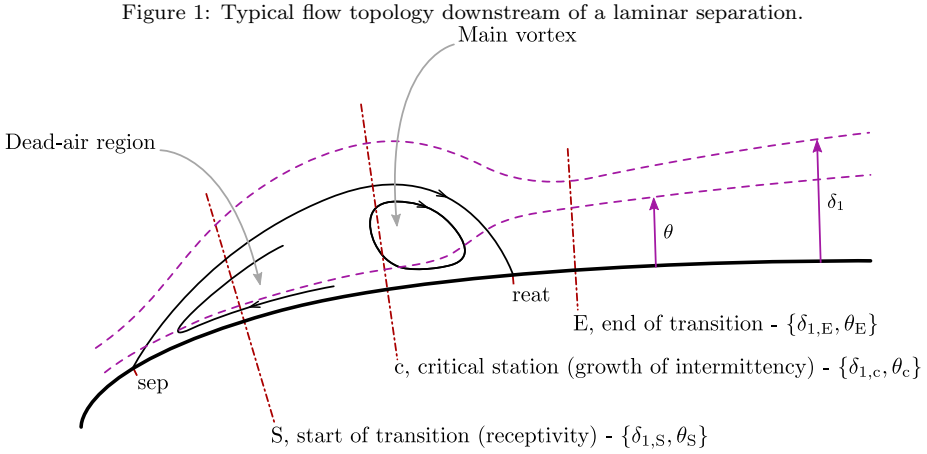

Studies aiming at understanding transition - separation-induced or otherwise - in wall-bounded flows have been accompanied by a significant modeling effort. Emmons (1951) [14] introduces a mathematical framework which has been widely accepted and used since, in which the final stage of transition is the creation of "turbulent spots", which propagate and spread through the boundary layer as they are advected, giving birth to the fully turbulent flow. This representation uses the concept of intermittency field, namely, the probability that the flow at given location and instant be turbulent through a range of realizations. Assuming a Dirac distribution of spots creation, Dhawan and Narasimha (1958) [15] supplement Emmons's equations with an estimation of the length of the transition zone and a shape to the intermittency function. This representation has paved the way to a simplification of the problem where the unknowns are reduced to the position of apparition of the first spots and the length of the transition zone. In order to determine these variables, the models rely heavily on empirical correlations between macroscopic properties of the flow, such as boundary-layer momentum thickness at the start of transition and freestream turbulence intensity, or pressure gradient parameter. The works of Roberts (1980) [16] and Hatman and Wang (1998) [17] deal specifically with separation-induced transition. The former will be further described in part 2.1 of the present paper.

These correlations can be used directly in a Reynolds-Averaged Navier-Stokes (RANS) computation, since they give a criterion to decide whether transition at a given point has started. These models have several drawbacks, however. First, they use integral variables of the boundary-layer, such as its momentum thickness, and therefore cannot straightforwardly reproduce some features of a two- or three-dimensional transition : when it starts, it does so on the whole thickness of the boundary layer, even though the sublayers can - and usually do - have different dynamics. Moreover, the computation of integral properties is nontrivial and costly in a parallel-computing environment. Its implementation in a Computational Fluid Dynamics (CFD) environment is also a complex task. Secondly, the use of these models is time-consuming and requires a high level of expertise, along with a previous knowledge of the flow topology. Thirdly, though a wide range of correlations have been published regarding the point at which transition starts (see table 2) [18–20], relatively few studies [21] have been aimed at defining the shape of the intermittency function and how turbulence must be produced, and Heaviside or Dhawan-Narasimha-like half-Gaussian distributions are often assumed. Finally, the use of transition criteria relies entirely on the hypothesis that transition processes do not interact. For example, it excludes the possibility of a main transition process driven by Kelvin-Helmholtz instabilities that amplify initial perturbations created by non-linear interactions between freestream turbulence and the boundary layer profile, as is often the case in turbomachinery flows. This assumption fails in numerous cases such as the "transitional" separation cases in the classification of Hatman and Wang. Despite these limitations, the transition criteria have been shown to provide accurate results for canonic flows on relatively simple geometries.

More recently, a different class of models that also make use of correlations has been proposed. These RANS models describe the transition properties as field variables, and feature additional transport equations to describe their dynamics . This approach, called correlations-based transition modeling, allows a far greater freedom for the shape of the transition zone. Notable works with this approach include those of Menter et al. (2006) [22] and Coder (2017) [23]. The

Amplification Factor Transport model by Coder (2017) [23] is natural transition-oriented, but the model devised by Langtry and Menter (2009) [24] claims to be able to take any type of transition into account and has been extended to reach this aim [25, 26]. This model has been thoroughly validated for a wide range of applications [27, 28]. Several transition models have been published that closely follow its philosophy and Langtry and Menter's method [29, 30]. The version of this model used here is more deeply described in part 2.2 and in appendix 7.1. The aim of the present paper is to assess the above-mentioned transition modeling strategies applied to the Spalart-Allmaras model [31] and to the $k-\omega-$SST model by Menter (1994) [32] for a laminar separation bubble test-case by Laurent et al. (2012) [33]. The paper is organized as follows. First, a further description of the correlations and transport equations used is provided. Then, the test-case is presented, along with some of the reference data. After an outlining of the numerical strategy adopted in the RANS computations, results are described, analyzed and compared to the reference in order to validate the use of the RANS models and gain a clear insight into their degree of accuracy and limitations.

2. Models description

2.1. Algebraic transition criteria

One of the most validated and used method to predict transition features is to use algebraic criteria that compute the onset of transition based on the boundary layer wall-normal profile. Transition criteria have been developed to properly model all types of transition [18–20, 34–37]. Most of these models seek to correlate the location of the onset of transition and its extent to the properties of the boundary layer, and specifically its history. Therefore, they make use of quantities that have been found to describe the state of the boundary layer best, such as its momentum thickness θ or its shape factor H. They also take into account properties of the external flow, such as the pressure gradient with

the Pohlhausen parameter λ_θ or the turbulence intensity.

While the turbulence equations are solved everywhere, allowing non-zero levels to the turbulence variables even in the laminar zones, their effect on the mean flow depends on the result of the transition criterion computation : if the boundary layer is declared laminar, the eddy viscosity is set to zero, otherwise it is computed from the turbulence variables. This means, for instance, that the eddy-viscosity is not necessarily continuous through the transition location. Catalano et al. (2015) [38] have underlined the paramount importance of solving the turbulence equations upstream of the transition point, especially in the dead-air region, for low-Reynolds number flows. While the current methods act on the eddy-viscosity rather than the turbulence production terms contrary to the advice of Catalano et al., their behavior in the laminar region seems to fulfil the requirements set in their study. The remaining difference in implementation between their advice and the current algebraic criterion models is assumed to have little influence, since the Reynolds number of the flow dealt with in this study is 1.8×10^6. Indeed, their study emphasizes quantitative differences for low Reynolds numbers (lower than 6.0×10^4), depending on the implementation, but also notes no significant difference for a higher Reynolds number flow (around the SD7003 airfoil at Reynolds number 6.0×10^6). This class of models has been applied successfully to the computation of transitional flows around airfoils with Reynolds numbers ranging from 5.0×10^4 to 2.5×10^5 in numerous previous studies, such as the development of the LSTT model by Bernardos et al. (2019) [39].

One notable criterion was first introduced by Abu-Ghannam and Shaw [19] for bypass transition. It correlates the momentum thickness-based Reynolds number $Re_\theta = \frac{\theta U_e}{\nu}$ at the start of transition, $Re_{\theta,\mathrm{S}}$, to the freestream turbulence intensity Tu and to the local pressure gradient parameter λ_θ. When the momentum thickness-based Reynolds number of the laminar boundary layer exceeds the correlated value of $Re_{\theta,\mathrm{S}}$, transition is declared started. The expression for this correlation is given further in table 2 and represented on figure 2. Since the correlation of $Re_{\theta,\mathrm{S}}$ by Langtry and Menter [24] is also used further and in

a slightly different context, it is also represented here for ulterior reference.
Since the test case used involves "short" separation-induced transition, the criterion of Roberts [16] is also used in order to take the effects of separation into account. This method links the distance between separation and transition to the freestream turbulence properties, assuming, for short laminar separation bubbles, that the transition location correlates well to the maximum displacement thickness abscissa of the boundary layer. Specifically, the distance between separation and transition is estimated using the intensity and macroscale length of turbulence. The reader is referred to ref. [16] for a more comprehensive and quantitative description of these formulae.

2.2. Local correlations-based transition models

Medida and Baeder (2011) [40] proposed a coupling method of the local correlations-based transition model (LCTM) developed by Langtry and Menter (2009) [24] to the turbulence model of Spalart and Allmaras (1992) [31]. Thus, two equations are added to the one-equation turbulence model, and these authors developped correlations to fit the experimental data used for calibrating the model. Both transport equations along with their components are the same as in the original Langtry-Menter model and are provided in appendix 7.1.

In the original model, the transition model is coupled to the evolution of the turbulence variables in two ways : first, the eddy-to-molecular viscosity ratio R_{T} intervenes in the source terms of the transition equations in eq. (11). Second, the production and destruction terms in the transport equations for k and ω are modified compared to those of the lone turbulence model. This coupling strategy was also adopted by Medida and Baeder.
Therefore, the transport equation for the modified eddy viscosity in the turbulence model by Spalart-Allmaras reads :

$$\mathrm{D}_t\tilde{\nu} = P_{\tilde{\nu}} - D_{\tilde{\nu}} + \frac{1}{\sigma}\sum_i \partial_{x_i}\left[\left(\nu + \tilde{\nu}\right)\partial_{x_i}\tilde{\nu}\right] + c_{\mathrm{b},2}\left(\partial_{x_i}\tilde{\nu}\right)^2 \tag{1}$$

where the Spalart-Allmaras working variable $\tilde{\nu}$ is defined from the eddy-viscosity ν_{t} :

$$\frac{\nu_{\mathrm{t}}}{\nu} = \chi f_{\mathrm{v},1} \text{ with } f_{\mathrm{v},1} = \frac{\chi^3}{\chi^3 + c_{\mathrm{v},1}^3} \text{ and } \chi = \frac{\tilde{\nu}}{\nu} \tag{2}$$

and the production and destruction terms, modified to take transition into account, read :

$$\begin{cases} P_{\tilde{\nu}} = \gamma_{\mathrm{eff}} c_{\mathrm{b},1} \tilde{\Omega} \tilde{\nu} \\ D_{\tilde{\nu}} = \min\left\{\max\left\{\gamma\ ;\beta\right\}\ ;1.0\right\} c_{\mathrm{w},1} f_{\mathrm{w}} \left(\frac{\tilde{\nu}}{d}\right)^2 \end{cases} \tag{3}$$

In this formulation, $\tilde{\Omega}$ is a modified vorticity magnitude :

$$\tilde{\Omega} = \Omega + \frac{\tilde{\nu}}{\kappa^2 d^2} f_{\mathrm{v},2} \text{ with } f_{\mathrm{v},2} = 1 - \frac{\chi}{1 + \chi f_{\mathrm{v},1}} \tag{4}$$

and the function f_{w} is defined as follows :

$$f_{\mathrm{w}} = g\left[\frac{1 + c_{\mathrm{w},3}^6}{g^6 + c_{\mathrm{w},3}^6}\right]^{\frac{1}{6}} \text{, where } g = r + c_{\mathrm{w},2}\left(r^6 - r\right) \text{ and } r = \frac{\tilde{\nu}}{\tilde{\Omega}\kappa^2 d^2} \tag{5}$$

In their study, Medida and Baeder use the so-called "rotational correction" by Dacles-Mariani et al. (1999) [41], which is a replacement of Ω by $\Omega + 2\min\left\{0\ ;S - \Omega\right\}$ in eq. (4). This correction aims at decreasing the production of $\tilde{\nu}$ in regions of flow where the vorticity magnitude exceeds the shear-stress. Its effects are assessed in this work.

β is a limiting factor preventing the destruction term to fall beneath a minimum rate of its turbulent value. γ_{eff} is an effective intermittency used in eq. (3), designed to overincrease the turbulence production if the flow separates :

$$\gamma_{\mathrm{eff}} = \max\left\{\gamma\ ;\gamma_{\mathrm{sep}}\right\} \tag{6a}$$

$$\gamma_{\mathrm{sep}} = \min\left\{s_1 \max\left\{\frac{Re_{\mathrm{v}}}{3.235\ Re_{\theta,\mathrm{c}}} - 1\ ;0\right\} F_{\mathrm{reattach}}\ ;2\right\} F_{\theta,\mathrm{t}} \tag{6b}$$

where

$$F_{\mathrm{reattach}} = e^{-\left(\frac{R_{\mathrm{T}}}{20}\right)^4} \tag{6c}$$

and

$$s_1 = 2,\ \beta = 0.5 \tag{6d}$$

Finally, the model is completed by the original Spalart-Allmaras constants, given in table 1.

Table 1: Calibration constants of the Spalart-Allmaras model [31].

Constant name	$c_{\mathrm{b},1}$	$c_{\mathrm{b},2}$	σ	$c_{\mathrm{w},1}$	$c_{\mathrm{w},2}$	$c_{\mathrm{w},3}$	$c_{\mathrm{v},1}$
Value	0.1355	0.622	$\frac{2}{3}$	$\frac{c_{\mathrm{b},1}}{\kappa^2} + \frac{1+c_{\mathrm{b},2}}{\sigma}$	0.3	2	7.1

The tripping functions $(f_{t,i})_{i\in\{1,2\}}$ initially included by Spalart and Allmaras are naturally omitted. Indeed, as their names indicate, they were only designed to obtain transition at a predefined desired location, which would be equivalent to imposing the transition location with vortex generators or a tripping line in an experiment.

2.3. Correlations

Special attention should be given to the $Re_{\theta,\mathrm{S}}$, F_{length} and $Re_{\theta,\mathrm{c}}$ variables, as they are the correlated functions upon which this class of models heavily rely. They represent the empirical part of the LCTM by Menter et al. [22] and introduce the link between the mathematical dynamic system and the physics of transition.

The first one, $Re_{\theta,\mathrm{S}}$, is the value of the momentum thickness-based Reynolds number at the location where the laminar boundary layer velocity profile would first become unstable and receptive to disturbances without turbulence model. This value is determined by a correlation. For the sake of coherence and simplicity, the notation adopted here is the one introduced by Abu-Ghannam and Shaw [19]. In this work, the expression given by Langtry and Menter [24] is used (see table 2). This correlation is plotted on figure 2, along with those of Abu-Ghannam and Shaw [19], Mayle [20] and Menter et al. [22] for several values of Tu_∞ and λ_θ. Even if one only considers the results for mildly adverse pressure gradients and moderately high values of turbulence intensity, there remains considerable differences between these correlations. Some might

Figure 2: Correlations for $Re_{\theta,\mathrm{S}}$, with λ_θ and Tu_∞ as variables published in [19], [20], [22] and [24].

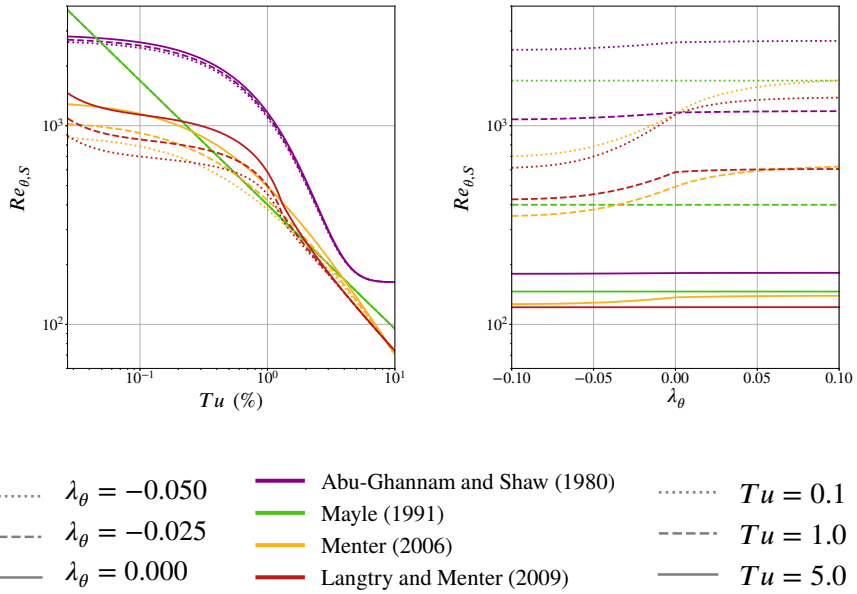

be explained through the context for which they were published. Furthermore, this study, exclusively based on two parameters, Tu_∞ and λ_θ, omits the already remarked-upon influence of other freestream turbulence parameters such as the eddy length scale [42].

$Re_{\theta,\mathrm{c}}$ is the Reynolds number based on the boundary layer momentum thickness at the station beyond which the intermittency starts to grow. F_{length} is an amplitude factor describing the rate of production of intermittency, and therefore the speed of transition and the length of the transition zone. These correlations, initially not included in the publication by Menter et al. [22], were eventually disclosed by Langtry and Menter [24]. However, significant effort had been made beforehand by other research teams to develop their own correlations. A number of existing and published correlations for $Re_{\theta,\mathrm{c}}$ and F_{length} are gathered in table 3. Medida and Baeder specifically designed new correlations for a Spalart-Allmaras framework.

Contrary to most correlations that have been published to fill in the gap left by Menter et al. , the Medida-Baeder correlations introduce a dependency of $Re_{\theta,\mathrm{c}}$ and F_{length} to the up- and freestream turbulence intensity as well as to the $Re_{\theta,\mathrm{t}}$ variable. Krause et al. [47] also used this process in the development of fitting correlations for the Menter et al. model. Both sets of correlations are represented on figure 3. Though they were not created for the same underlying turbulence model, their common role is to describe the point of transition onset and the speed of the transition process, making the comparison qualitatively relevant. The F_{length} correlation of Krause et al. was evaluated for a typical $Re_{\theta,\mathrm{t}}$ of 1000. It can be easily verified that the shape of this function does not depend on $Re_{\theta,\mathrm{t}}$ and that this representation allows for a justified comparison. For the sake of completeness, the correlations by Medida and Baeder are plotted against a wide range of freestream turbulence intensities. It should be noted however, that they were developed with a low turbulence intensity context in mind, and, as is obvious upon seeing the figure, are not valid beyond $Tu = 0.7\,\%$ (though the authors mention a limit of applicability as high as $1\,\%$). Specifically, the model predicts a diverging value for $Re_{\theta,\mathrm{c}}$ as Tu_∞ becomes large, delaying transition, or even preventing it altogether, which is contrary to the physics of bypass transition.

Figure 3: Empirical correlations developed in [40] and [47] for the onset of transition and the extent of the transition zone in a $\gamma - Re_{\theta,\mathrm{t}}$ transition model.

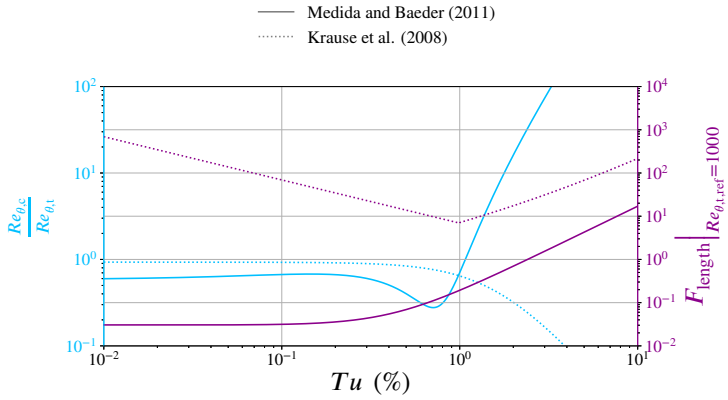

Table 2: Some empirical correlations linking $Re_{\theta,\mathrm{S}}$ to the global properties of a transitional flow.

Author(s)	Year	Correlated value for $Re_{\theta,\mathrm{S}}$	Auxiliary functions	Complements and limits
Seyb [18]	1967	$\frac{1000}{1.2+0.7\ Tu}+10\left(\frac{0.09+\lambda_\theta}{.0106+0.036\ Tu}\right)^{2.62}$		$Tu\in[0.1,4]$
Dunham [43]	1972	$\left(0.27+0.73\ e^{-.8\ Tu}\right)\left(550+\frac{680}{1+Tu-21\ \lambda_\theta}\right)$		
Hall and Gibbings [44]	1972	$190+e^{6.88-1.03\ Tu}$		
Abu-Ghannam and Shaw [19]	1980	$163+e^{6.91-Tu}\exp\left[\frac{F_{\mathrm{Abu-Ghannam}}(\lambda_\theta)}{6.91}\right]$	$F_{\mathrm{Abu-Ghannam}}(\lambda_\theta)=\begin{cases}6.91+12.75\ \lambda_\theta+63.64\ \lambda_\theta^2 & \text{if } \lambda_\theta\le 0\\ 6.91+2.48\ \lambda_\theta-12.27\ \lambda_\theta^2 & \text{if } \lambda_\theta>0\end{cases}$	
Hourmouziadis [45]	1989	$460\ Tu^{-.65}$		
Mayle [20]	1991	$400\ Tu^{-\frac{5}{8}}$		
Suzen et al. [37]	2002	$\left(120+150\ Tu^{-\frac{5}{8}}\right)\coth\left[4\left(0.3-10^5\ K\right)\right]$		
Menter et al. [22]	2006	$803.73\left(Tu+0.6067\right)^{-1.027}F_{\mathrm{Menter}}\left(Tu,\lambda_\theta,K\right)$	$F_{\mathrm{Menter}}\left(Tu,\lambda_\theta,K\right)=\begin{cases}1+\left(1.32\ \lambda_\theta+89.47\ \lambda_\theta^2+265.51\ \lambda_\theta^3\right)e^{-\frac{Tu}{3}} & \text{if } \lambda_\theta\le 0\\ 1+\left[.0962\left(K\cdot 10^6\right)+0.148\left(K\cdot 10^6\right)^2+0.0141\left(K\cdot 10^6\right)^3\right]\left[1-e^{-\frac{Tu}{1.5}}\right] & \\ \quad+0.556\left(1-e^{-23.9\ \lambda_\theta}\right)e^{-\frac{Tu}{1.5}} & \text{if } \lambda_\theta>0\end{cases}$	$\begin{cases}\lambda_\theta\in[-0.1,0.1]\\ K\in[-3,3]\cdot 10^{-6}\\ Re_{\theta,\mathrm{S}}\ge 20\end{cases}$
Langtry [46]	2006	$\begin{cases}\left(1173.51-589.428\ Tu+\frac{0.2196}{Tu^2}\right)F_{\mathrm{Langtry}}\left(Tu,\lambda_\theta\right) & \text{if } Tu\le 1.3\\ 331.50\left(Tu-0.5658\right)^{-.671}F_{\mathrm{Langtry}}\left(Tu,\lambda_\theta\right) & \text{if } Tu>1.3\end{cases}$	$F_{\mathrm{Langtry}}\left(Tu,\lambda_\theta\right)=\begin{cases}1+\left(12.986\ \lambda_\theta+123.66\ \lambda_\theta^2+405.689\ \lambda_\theta^3\right)e^{-\left(\frac{Tu}{1.5}\right)^{1.5}} & \text{if } \lambda_\theta\le 0\\ 1+0.275\left(1-e^{-35\ \lambda_\theta}\right)e^{-\frac{Tu}{0.5}} & \text{if } \lambda_\theta>0\end{cases}$	$\begin{cases}Tu\ge 0.027\\ \lambda_\theta\in[-0.1,0.1]\\ Re_{\theta,\mathrm{S}}\ge 20\end{cases}$

Table 3: Some published correlations for the closure of $\gamma - Re_{\theta,\mathrm{t}}$ models.

Authors	Application range and recommendations	F_{length}	$Re_{\theta,\mathrm{c}}$
Krause et al. (2008) [47]	subsonic flat plates and hypersonic bodies, $Tu_\infty \in [0.18, 6.6]\,\%$	$\begin{cases} \dfrac{\ln(1+Re_{\theta,\mathrm{t}})}{Tu_\infty} & \text{if } Tu_\infty \leq 1\% \\ \left(2.1449 - 1.3493\ Tu_\infty + 0.2337\ Tu_\infty^2\right)\ln(1+Re_{\theta,\mathrm{t}}) & \text{if } Tu_\infty > 1\% \end{cases}$	$\dfrac{Re_{\theta,\mathrm{t}}}{1.0744+0.0118\ Tu_\infty+0.4233\ Tu_\infty^2-0.042\ Tu_\infty^3}$
Langtry and Menter (2009) [24]	bypass, natural and separation-induced transition, $Tu_\infty \geq 0.1\%$	$F_{\mathrm{length,base}}\left(1-F_{\mathrm{sublayer}}\right)+40\ F_{\mathrm{sublayer}}$, with : $F_{\mathrm{sublayer}} = e^{-\left(\frac{Re_\omega}{0.4}\right)^2}$ $F_{\mathrm{length,base}} = \begin{cases} 398.189\cdot10^{-1} - 119.270\cdot10^{-4}\ Re_{\theta,\mathrm{t}} - 132.567\cdot10^{-6}\ Re_{\theta,\mathrm{t}}^2 & \text{if } Re_{\theta,\mathrm{t}} < 400 \\ 263.404 - 123.939\cdot10^{-2}\ Re_{\theta,\mathrm{t}} + 194.548\cdot10^{-5}\ Re_{\theta,\mathrm{t}}^2 - 101.695\cdot10^{-8}\ Re_{\theta,\mathrm{t}}^3 & \text{if } 400 \leq Re_{\theta,\mathrm{t}} < 596 \\ 0.5 - 3\cdot10^{-4}\ (Re_{\theta,\mathrm{t}} - 596) & \text{if } 596 \leq Re_{\theta,\mathrm{t}} < 1200 \\ 0.3188 & \text{if } 1200 \leq Re_{\theta,\mathrm{t}} \end{cases}$	$\begin{cases} Re_{\theta,\mathrm{t}} - 396.035\cdot10^{-2} + 12.656\cdot10^{-4}\ Re_{\theta,\mathrm{t}} - 868.230\cdot10^{-6}\ Re_{\theta,\mathrm{t}}^2 + 696.506\cdot10^{-9}\ Re_{\theta,\mathrm{t}}^3 - 174.105\cdot10^{-12}\ Re_{\theta,\mathrm{t}}^4 & \text{if } Re_{\theta,\mathrm{t}} \leq 1870 \\ Re_{\theta,\mathrm{t}} - 593.11 - 0.482\,(Re_{\theta,\mathrm{t}} - 1870) & \text{if } Re_{\theta,\mathrm{t}} > 1870 \end{cases}$
Suluksna et al. (2009) [48]	bypass and separation-induced transition in flows submitted to adverse pressure gradient and high freestream turbulence intensity	$\min\left\{300\,;0.45+0.1\exp\left(12-0.022\ Re_{\theta,\mathrm{t}}\right)\right\}$	$\min\left\{Re_{\theta,\mathrm{t}}\,;\max\left\{125\,;-120+1.47\ Re_{\theta,\mathrm{t}}-(0.025)^2\ Re_{\theta,\mathrm{t}}^2\right\}\right\}$
Content and Houdeville (2010) [49]	low turbulence intensity $\sigma_{\theta,\mathrm{t}} = 10$	$\exp\left(2.5652 + 8.16\cdot10^{-3}\ Re_{\theta,\mathrm{t}} + 7.42\cdot10^{-6}\ Re_{\theta,\mathrm{t}}^2 - 1.325\cdot10^{-8}\ Re_{\theta,\mathrm{t}}^3\right)$	$Re_{\theta,\mathrm{t}}\min\left\{1\,;0.849 - 1.228\cdot10^{-3}\ Re_{\theta,\mathrm{t}} + 1.623\cdot10^{-6}\ Re_{\theta,\mathrm{t}}^2\right\}$
Content (2011) [50]	natural transition, $Tu_\infty \leq 1\%$	$\max\left\{10^{-4}\,;\exp\left(1.98 - 1.423\cdot10^{-3}\ Re_{\theta,\mathrm{t}}\right)\right\}$	$Re_{\theta,\mathrm{t}}\min\left\{1\,;0.8779 - 3.4\cdot10^{-4}\ Re_{\theta,\mathrm{t}} + 1.227\cdot10^{-7}\ Re_{\theta,\mathrm{t}}^2\right\}$
Medida and Baeder (2011) [40]	natural to mild bypass transition, $Tu_\infty \leq 1$, Spalart-Allmaras' model	$0.0306 - 0.0083\ Tu_\infty + 0.171\ Tu_\infty^2$	$\left(0.585 + 1.37\ Tu_\infty - 5.7\ Tu_\infty^2 + 4.45\ Tu_\infty^3\right) Re_{\theta,\mathrm{t}}$
Minot et al. (2015) [51] A	bypass and separation-induced transition in turbomachinery : high Tu_∞ and highly negative λ_θ	$1235 + 3.532\ Re_{\theta,\mathrm{t}} - 3.547\cdot10^{-3}\ Re_{\theta,\mathrm{t}}^2$	$\left(0.7754 - 6.810\cdot10^{-4}\ Re_{\theta,\mathrm{t}} + 6.516\cdot10^{-7}\ Re_{\theta,\mathrm{t}}^2\right) Re_{\theta,\mathrm{t}}$
Minot et al. (2015) [51] B	see Minot et al. [51] A. $s_1 = 10$ for improved separation prediction	$1129 + 4.260\ Re_{\theta,\mathrm{t}} - 5.03\cdot10^{-3}\ Re_{\theta,\mathrm{t}}^2 + 7.949\cdot10^{-7} Re_{\theta,\mathrm{t}}^3$	$\left(0.9472 - 6.095\cdot10^{-4}\ Re_{\theta,\mathrm{t}} + 6.578\cdot10^{-7}\ Re_{\theta,\mathrm{t}}^2\right) Re_{\theta,\mathrm{t}}$
Minot (2016) [52]	see Minot et al. [51] A. Smith model [53]	$\max\left\{10^{-4}\,;177.1 + 2.66\ Re_{\theta,\mathrm{t}} - 5.441\cdot10^{-2}\ Re_{\theta,\mathrm{t}}^2 + 3.7\cdot10^{-5}\ Re_{\theta,\mathrm{t}}^3\right\}$	$\left(0.9164 - 8.352\cdot10^{-4}\ Re_{\theta,\mathrm{t}} + 1.266\cdot10^{-6}\ Re_{\theta,\mathrm{t}}^2\right) Re_{\theta,\mathrm{t}}$

3. Test case description

3.1. Simulation methods

The RANS models described in section 2 and implemented in the elsA software [54] were applied to the flat-plate zonal Direct Numerical Simulation (DNS) test case of Laurent et al. (2012) [33]. This academic configuration was designed to mimic the pressure gradient of the OA209 airfoil profile with a 15°-angle of attack [55]. As the angle of attack is increased, the profile experiences leading edge separation due to the adverse pressure gradient shortly before deep stall. The laminar separation bubble allows a fast transition of the boundary layer, which reattaches.

In order to gain better understanding of the OA209 case, Laurent et al. designed a canonic test case that independently addresses the problem of separation-induced transition. Their configuration aims at discarding the effects of the pressure gradient after reattachment, of surface curvature, and of information coming from the trailing edge as well as perturbations from the leading edge of the airfoil. This approach had already received some amount of attention with other works [5, 7, 56, 57].

The geometry used here, presented on figure 4, is comprised of a zero-thickness flat plate faced by an opposite curved slipping wall. The curvature of the latter was iteratively computed by Laurent et al. to fit the pressure gradient distribution of the OA209 airfoil, starting from an inviscid estimation and using fully turbulent computations. The coordinates of the upper wall are given in *annexe* F.2 of ref. [58]. Moreover, and contrary to the experimental studies of the other authors mentioned above, Laurent et al. chose to let the turbulent reattached boundary layer develop under zero-pressure gradient conditions. Therefore, the domain of interest, containing the recirculation bubble, opens on a wide section containing both the turbulent boundary layer zone and a high freestream zone where the injection at the inlet boundary condition was designed to create no free shear layer from the junction downstream. This process prevents an interaction between the free shear layer and the developing turbulent boundary

Figure 4: Mesh used for the RANS simulations. Every node at the boundary conditions and one mesh line in four are plotted.

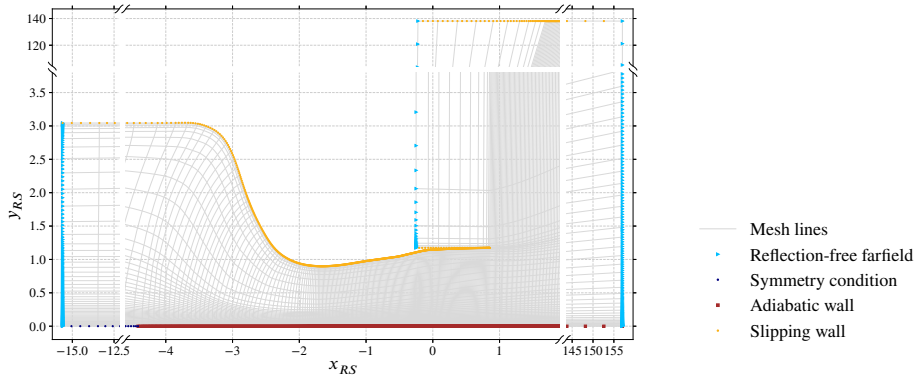

layer.

Special attention should be paid to the zonality of the computation : Laurent et al. only performed a DNS on the part of the domain surrounding the laminar-separation bubble.

3.2. Conditions and main features of the reference flow

The flow conditions of the OA209 airfoil near stall were used for the DNS : based on a chord length of 1 m, a freestream Reynolds number of 1.8×10^6 is imposed. The freestream Mach number is 0.16.

The main features of the reference flow can be seen on figure 5. As the flow separates from the flat plate, a recirculation is formed, where the maximum reverse flow velocity norm reaches 13 % of the freestream velocity norm. In the following, a new set of coordinates (x_{RS}, y_{RS}) is defined :

$$x_{RS} = \frac{x - x_{\text{reat}}^{\text{DNS}}}{x_{\text{reat}}^{\text{DNS}} - x_{\text{sep}}^{\text{DNS}}},\ y_{RS} = \frac{y}{x_{\text{reat}}^{\text{DNS}} - x_{\text{sep}}^{\text{DNS}}} \tag{7}$$

The shear layer formed through separation allows a fast transition [33]. The production of turbulence forces reattachment, forming a "short" laminar separation bubble (in the sense of [12]). The maximum distance from the streamline separating the external mean flow and the recirculating one to the wall amounts

Figure 5: Reference flow and boundary-layer thicknesses from the zonal DNS computations by Laurent et al.

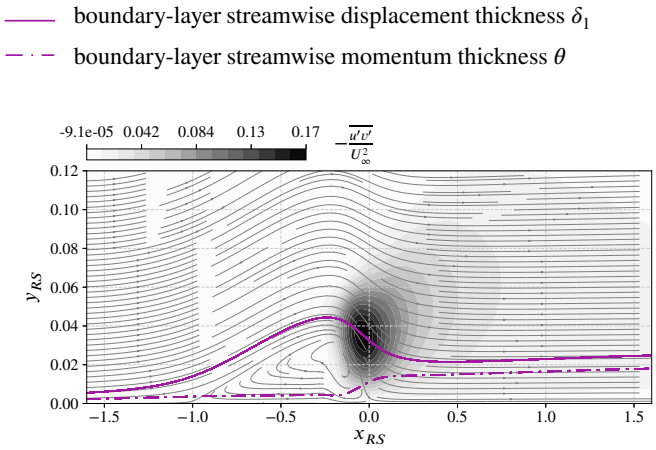

to 3.5 % of the distance L_{RS} between the separation and the reattachment locations. Due to the design of the upper injection values, no free shear layer is formed as the reattached flow reaches the open cavity. In this zero-pressure gradient zone, a fully turbulent boundary layer develops over the flat plate.

4. Numerical apparatus

4.1. Mesh and boundary conditions

The geometry used includes the wide cavity downstream of reattachment as in [33]. All meshes used for the RANS computations are two-dimensional, and a mesh convergence procedure is followed to ensure mesh-independence of the solution in the transition region. The influences of mesh refinement in both directions were examined, and we present the results obtained regarding streamwise mesh distribution. The fineness of the mesh in the streamwise direction in the transition region is represented by the wall-unit value Δx^+ of mesh spacing at the station $x_{RS} = -\frac{1}{2}$, which cuts the DNS separation bubble vertically at its middle point between separation and reattachment. As the separation location given by all RANS models is in good agreement with the value observed in the DNS, $x_{RS} = -\frac{1}{2}$ is a critical region for the model in all computations. Values of the grid spacing ratio $\frac{\Delta x^+}{\Delta y^+}$ ranging from 8 to 330 at this location were used. A uniform wall-normal grid spacing along the length of the flat plate was chosen. In order to obtain maximum values below 1 for Δy^+ in the fully turbulent boundary-layer as far as $13L_{RS}$ dowstream of reattachment, the chosen wall-normal grid spacing value amounts to $\Delta y^+ \in [0.1, 0.3]$ at $x_{RS} = -\frac{1}{2}$ where the skin friction is lower than in the turbulent region. Therefore, the range of Δx^+ used in the streamwise grid convergence study is $[0.9, 100]$. These values start from quasi-DNS resolutions. The upper bound, though lower than the values typically found in RANS computations, is sufficient to produce malfunctioning of the models and was therefore deemed sufficient to demonstrate the necessity of a fine mesh in the transitional region - based on fully-turbulent flow criteria. This study therefore thoroughly assesses the robustness of the Langtry-Menter model to streamwise mesh refinement for a simple separation-induced transition test-case. Indeed, the sensitivity of this model to mesh distribution has been reported [59]. The evolution of the skin-frition coefficient with mesh fineness is represented on figure 6.

Figure 6: Skin-friction coefficient obtained with the $\tilde{\nu} - \gamma - Re_{\theta,\mathrm{t}}$ model as the longitudinal refinement of the mesh is increased.

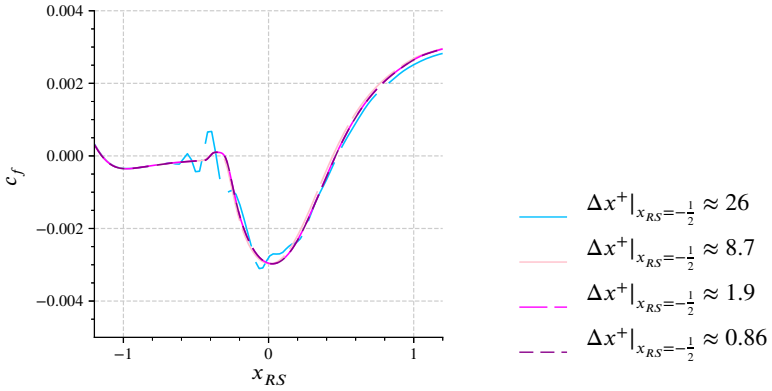

It is seen that the resolution required to obtain convergence is significantly higher than usual recommendations for RANS computations such as $\Delta x^+ \approx 400$. However, it must be kept in mind that the skin friction in the transitional region is significantly lower than in a fully turbulent boundary layer. The hypotheses underlying the usual recommendations are therefore of a questionable validity here. In order to check whether the observed requirement is an intrinsic property of the model or if the nature of the test case plays a dominant part in it, the same set of computations was realized using the $k - \omega$ SST model as basis for the Langtry-Menter transition model, as originally proposed by its authors [24]. The same evolution was observed with the same critical values for Δx^+ in the center of the bubble. Therefore, the pathological behavior observed when Δx^+ at $x_{RS} = -\frac{1}{2}$ is increased beyond 10 does not appear to be caused specifically by the coupling to the Spalart-Allmaras model, but, to the contrary, it seems to stem from the Langtry-Menter model itself. It must be emphasized that an influence of the mesh on the flow is to be expected when the cell length is not small enough to allow a proper discretization of the separated region where the transition is quite abrupt. Table 4 reports several values deemed worthy of interest in the computations. This study gives an insight into the streamwise grid-spacing requirements of the Langtry-Menter model applied either to

the Spalart Allmaras model or to the $k-\omega$ SST model for separation-induced transition : $\Delta x^+ = 10$ in the vicinity of the transition location appears to be an upper bound to ensure both mesh independence and the proper working of the model.

Since the flow does not appear to undergo significant changes when Δx^+ is reduced below 8.7 at $x_{RS} = -\frac{1}{2}$, the mesh with $\Delta x^+ = 1.9$ at this location was considered refined far beyond what is necessary to ensure mesh independence and prove the robustness of the model to refinement. The data presented further therefore results from computations using this mesh.

Table 4: Mesh-related properties of the mesh convergence computations using the Spalart-Allmaras-$\gamma - Re_{\theta,\mathrm{t}}$ model.

Δx^+ at $x_{RS} = -\frac{1}{2}$	Unsteady flow	Number of grid nodes at the wall in the separated region	Relative length of the laminar separation bubble compared to DNS
64	yes	-	-
26	yes	69	1.64
8.7	no	87	1.59
4.2	no	184	1.61
1.9	no	394	1.61
0.86	no	879	1.61

An analogous procedure regarding the wall-normal discretization parameters was followed, finally producing the mesh upon which the following results were obtained. This mesh is comprised of 552 992 cells.

The height of the first cell at the wall nears 1×10^{-6} m in the vicinity of the bubble and 5×10^{-6} m in the fully turbulent boundary layer, amounting to a maximum Δy^+ value of 0.6. A schematics of the zone of interest can be seen on

figure 4. Note that the domain is shortened through omission of substantial slices and compression of scales at the right-, left- and upper-borders. Non-reflective strategies are used for inlet and exit conditions, using the reference-state values summarized in table 5. The use of a similar state for both the upper inlet and the outlet is justified by the vastly greater height of the upper zone compared to that of the boundary layer and the lower zone. Therefore, the contribution of the flux of conservative variables through the lower zone to the flux through the exit is negligible. A weak inlet turbulence intensity of roughly 0.01 % is imposed.

The compressible fluid is assumed to be a perfect gas with constant Prandtl number and Laplace coefficient, obeying Sutherland's law.

Viscous fluxes are computed using the AUSM+P scheme [60]. Furthermore, convergence is achieved through an implicit backward Euler time-marching process, with a local timestep method and a Courant-Friedrichs-Lewy (CFL) number of 4. The convergence of the implicit computations is accelerated using the LU-SSOR scalar spectral radius method.

4.2. Models

For the sake of meaningful comparisons, both the $k-\omega-\gamma-Re_{\theta,\mathrm{t}}$ model by Langtry and Menter [24], based on the $k-\omega-$SST turbulence model by Menter (1994) [32], and the $\tilde{\nu}-\gamma-Re_{\theta,\mathrm{t}}$ model previously described [40] are used. Moreover, computations are run using the transition criterion by Roberts [16]. These computations allow a thorough evaluation of the influence of the $\gamma-Re_{\theta,\mathrm{t}}$ framework on the behavior of the turbulence models, and some measure of assessment of the errors due to the transition modeling stategies as opposed to the errors induced by the turbulence model itself. The $\gamma-Re_{\theta,\mathrm{t}}$ transition modeling strategy applied to the Spalart-Allmaras turbulence model is used first without modification of Ω. Results obtained using the Dacles-Mariani correction are also presented. Finally, some conclusions are drawn by modifying the model's correlations and using those of Langtry and Menter, initially designed for a $k-\omega$

Table 5: Reference state values (IS units) at both inlet boundaries and at outlet. Turbulent variables are given for all models and are only used when applicable.

Field name	Symbol	Bottom inlet	Top inlet, outlet
Density	ρ	1.22	1.13
Momentum : x-component	ρu_x	57.85	154.05
Momentum : y-component	ρu_y	0	
Momentum : z-component	ρu_z	0	
Energy stagnation density	ρe	255 125	239 984
Modified eddy-viscosity density	$\rho\tilde{\nu}$	1.8×10^{-7}	
Turbulent kinetic energy density	ρk	5.49×10^{-5}	
Turbulent specific dissipation rate density	$\rho\omega$	3689	
Intermittency density	$\rho\gamma$	1.22	
Momentum thickness-based Reynolds number	$\rho Re_{\theta,\mathrm{t}}$	1137	

turbulence model.

5. Results and discussion

5.1. Criterion and transport equations framework

The first comparisons involve both $\gamma - Re_{\theta,\mathrm{t}}$ models and both criterion computations. f_{w} and $P_{\tilde{\nu}}$ are computed using Ω. Maps of the cross components of the turbulence shear-stress tensor are plotted on figure 7. All RANS models build a separation bubble, and the separation location is insensitive to both turbulence- and transition-modeling, indicating non-interference of the RANS model in the laminar-zones computations. However, the dimensions of the separated region are always overestimated : the RANS separation bubbles are both

Figure 7: Reynolds turbulence shear stress cross components fields obtained with $\gamma - Re_{\theta,\mathrm{t}}$ models and the Roberts algebraic transition criterion.

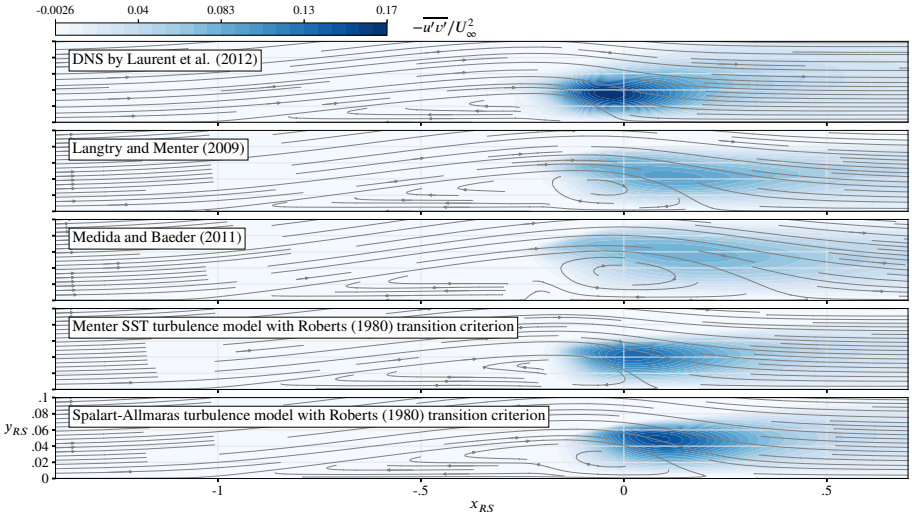

too long and too thick. This global failure to estimate the correct bubble dimensions can be explained by an analysis of the turbulence production. Because of an underestimation of the turbulence production in the zone immediately aft of the transition location, no RANS computation reaches the reference values for the main turbulence shear stress. In this regard, the Roberts algebraic criterion-based models yield better predictions than the $\gamma - Re_{\theta,\mathrm{t}}$ models, but they also display this behavior to a lesser extent. In all cases, the pressure recovery induced by turbulence production is slowed by this weakened activation, and reattachment is delayed. More quantitatively, the separating streamlines for each flow are plotted on figure 8, with a color scheme of figures that is used for all results of this four-model comparison. The separating streamlines presented on figure 8, issued from the stagnation points in the flow, define statistically closed regions : in average, fluid particles inside one of these lines will stay inside. Note that the determination of these streamlines is highly subject to integration imprecision, accounting for the fact that most lines do not exactly stop at the wall. Both an upper and lower estimation of their position have been plotted, which is quite sufficient for the current discussion. The bubble

lengths are overestimated by as much as 50 % in the case of the $\tilde{\nu} - \gamma - Re_{\theta,\mathrm{t}}$ model, and in all cases by at least 10 %. The wall-normal thickness of the recirculation region is overestimated respectively by 35, 85, 15 and 30 % using resp. the $k - \omega - \gamma - Re_{\theta,\mathrm{t}}$, the $\tilde{\nu} - \gamma - Re_{\theta,\mathrm{t}}$, the $k - \omega$-Roberts and the Spalart-Allmaras-Roberts model. Furthermore, the flow obtained with Spalart and Allmaras' model complemented with a $\gamma - Re_{\theta,\mathrm{t}}$ approach exhibits a sufficiently overestimated separated zone for a secondary recirculation to appear between the main vortex and the dead-air region.

Figure 8: Flow-separating streamlines obtained with $\gamma - Re_{\theta,\mathrm{t}}$ models and the Roberts algebraic transition criterion. The same legend is used in figures 9, 10 and 11.

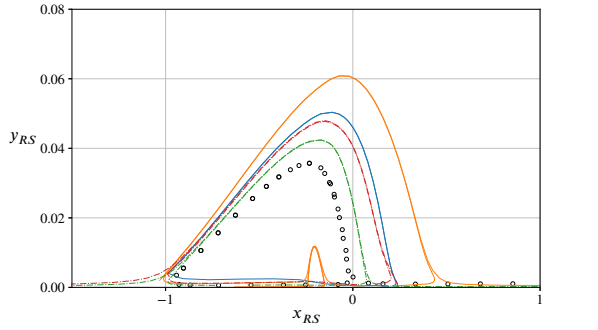

More quantitatively, the evaluation of the Reynolds shear stress components along several wall-normal lines in internal units inside the recirculation zones leads to figure 9. The delay in the increase of turbulence from the transition point downstream is noticeable in two facts : first, most RANS models build a maximum amplitude of Reynolds shear stress cross-components in slices $(3-4)$, while the averaged DNS flow exhibits a maximum in slice (2), and second, the

decrease in turbulence occurs early in the DNS compared to RANS : along all slices from slice (4) downstream, $-\overline{u'v'}/U_\infty^2$ reaches higher values in RANS computations than in the reference flow. While the wall-normal position of the highest production of turbulence is, for all models, overestimated, this bias can be attributed to an overall large thickness of the laminar separation bubble. Presumably, reducing that thickness and therefore decreasing the distance between the wall and the main shear region would also amount to a smaller distance of the main turbulence production region to the wall. More disturbing, however, is the relatively timely first increase of turbulence given by the $\gamma - Re_{\theta,\mathrm{t}}$ models : in slice (1), the flows obtained using these models show a level of turbulence shear stress similar to that of the reference flow, whereas its growth is too slow. Indeed, though with a late start, the $k-\omega$ model together with Roberts' criterion reaches the maximum value of turbulence shear stress cross components with the best accuracy. This might indicate a failure of the $\gamma - Re_{\theta,\mathrm{t}}$ framework to reproduce a brutal transition mechanism despite the overincrease of γ_{eff} in a separated region, or an insufficient action on the part of the γ_{sep} correction.

Figure 10 represents the evolution of integral boundary-layer variables along the wall. All the tested RANS models produce an overestimation of the boundary layer displacement thickness δ_1, while the momentum thickness θ is better captured, giving rise to an increase in shape factor H in the separated region. Again, it is seen that the criterion-based transition strategies perform better than turbulence models supplemented with $\gamma - Re_{\theta,\mathrm{t}}$ transport equations. It is also clear that the behavior of the $k-\omega-\mathrm{SST}$ turbulence model allows a better reproduction of the physics of the separated boundary layer. Combined with our previous remark that the flows obtained with the model by Spalart-Allmaras show a higher level of turbulence shear-stress, this observation leads to a conclusion : the overall level of turbulence must not be the most important criterion at play in the shape of the separation bubble. Since the flow with the $k-\omega-\mathrm{SST}$ model also exhibits an earlier first rise in turbulence, it can be inferred that accurately computing the location of the first increase in Reynolds'

Figure 9: Reynolds turbulence shear stress cross-components profiles obtained along the wall-normal lines $x_{RS} = -0.2$ (1), -0.05 (2), 0.1 (3), -0.25 (4), 0.4 (5), 0.7 (6), 1 (7) with $\gamma - Re_{\theta,\mathrm{t}}$ models and the Roberts algebraic transition criterion.

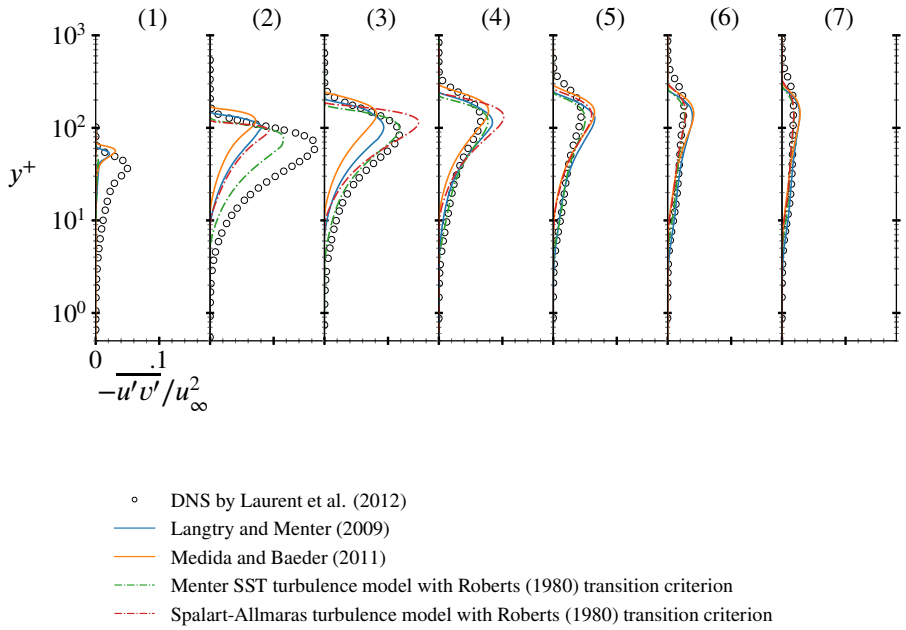

stresses is more crucial than estimating its global amplitude.

In addition to our previous statements about the weak turbulence production by the $\tilde{\nu} - \gamma - Re_{\theta,\mathrm{t}}$ model, it must also be noted that the asymptotic friction coefficient is underestimated in the fully-developed turbulent boundary layer with this model, creating a default in the slope of the momentum thickness. Moreover, both transition models associated with the $\tilde{\nu}$ model fail to build the excess of friction after reattachment compared to the asymptotic boundary layer, while both models based on the turbulence model by Menter develop it to some extent.

Figure 11 aims at evaluating the ability of the models to build a canonic boundary layer profile in the fully turbulent zone downstream of reattachment, comprised of the internal, the buffer and the external layers. To that effect, the

asymptotic laws of the turbulent boundary layer are also plotted. As expected, the boundary layer slightly downstream of the DNS-flow reattachment is highly modified by the late RANS reattachments, and the log-layer profile that is already apparent in the flow of the DNS at stations $(1')$ and $(2')$ only appears from the station $(3')$ downstream for the flows obtained with $\gamma - Re_{\theta,\mathrm{t}}$ models and from the station $(2')$ downstream for the flows obtained with Roberts' criterion. In the fully turbulent boundary layer at stations $(3' - 5')$, a better agreement is observed, though with some delay due to the overall lateness of the starts of transition given by the RANS models. Therefore, the $\gamma - Re_{\theta,\mathrm{t}}$ framework applied to Spalart and Allmaras' model qualitatively preserves the ability of the turbulence model to behave nominally in a turbulent boundary layer. However, it will be seen in part 5.3 that the transition model jeopardizes the quantitative recovery of the fully-turbulent behavior.

Figure 10: Boundary-layer 1-dimensional variables obtained with $\gamma - Re_{\theta,\mathrm{t}}$ models and the Roberts algebraic transition criterion. (a) : streamwise displacement thickness, (b) : streamwise momentum thickness, (c) : shape factor, (d) : skin friction coefficient.

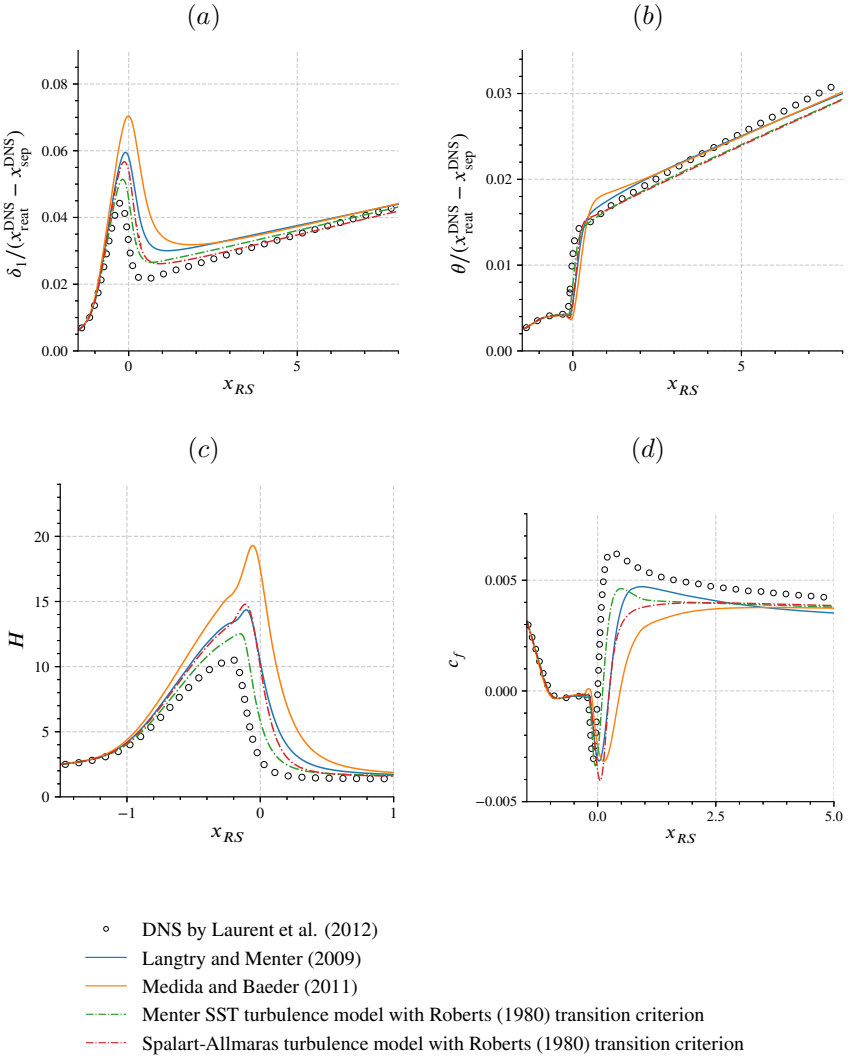

Figure 11: Velocity profiles obtained along the wall-normal lines $x_{RS} = 0.25$ $(1')$, 0.5 $(2')$, 2 $(3')$, 4 $(4')$, 6 $(5')$ with $\gamma - Re_{\theta,\mathrm{t}}$ models and the Roberts algebraic transition criterion.

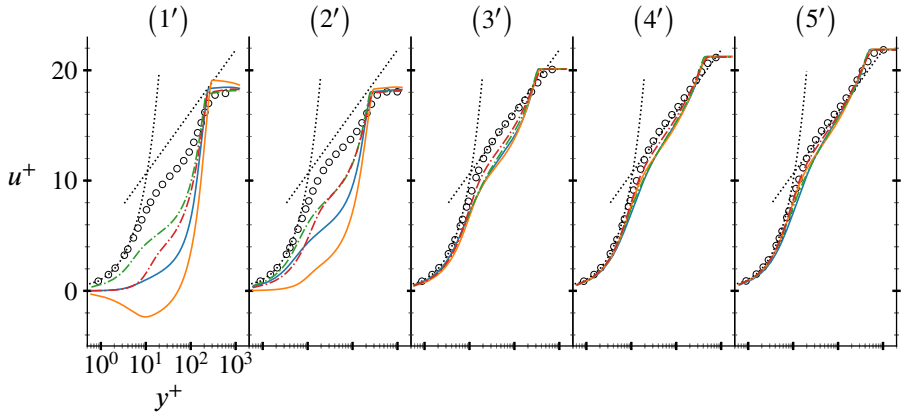

Figure 12: Activation zones of the modification by Dacles-Mariani et al. of the source terms in Spalart and Allmaras' model.

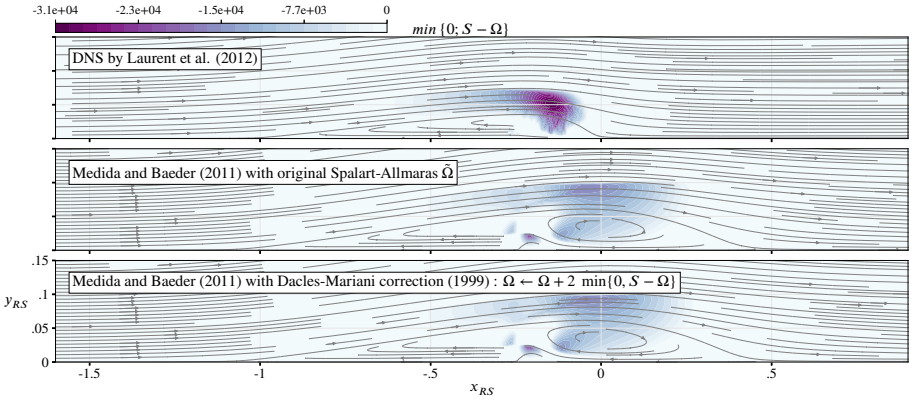

5.2. Modification of the turbulence production term

The following part deals with the effects of modifying the vorticity scale in the production and destruction terms of the Spalart-Allmaras model. This modification replaces Ω with $\Omega + 2\min\{0\ ; S-\Omega\}$ in the computation of $\tilde{\Omega}$ (see eq. (4)), as is the case in Medida and Baeder's study. It is observed that :

$$\Omega \geq \Omega + 2\min\{0\ ; S-\Omega\} = \begin{cases} \Omega & \text{where the fluid rotates less than it is sheared,} \\ 2\ S-\Omega & \text{everywhere else.} \end{cases} \tag{8}$$

This reformulation emphasizes that the model's correction comes in play when the flow is submitted to a stronger rotation than shear, in which case $\tilde{\Omega}$ is decreased, inducing an increase in destruction and a drop of production. The zones where this correction is activated appear dark on figure 12, along with the general flow topology. Interestingly, these locations of highly negative value for $\min\{0\ ; S-\Omega\}$ in the reference flow do represent locations where an increase in turbulence production could be desired in this case. However, in most cases, regions of strong rotation with eddies that have a high length scale tend to be weaker generators of turbulence than highly-sheared regions, which explains why the proposed correction decreases turbulence in regions where the rotation

dominates the strain rate. The use of the modification by Dacles-Mariani et al. in Medida and Baeder's model only has a marginal effect on the flow, small enough as to not be worth developing much further. This effect does not correct the lack of turbulence production previously observed, quite the opposite (which is in agreement with its intended working). The production being decreased in the transition zone, the bubble is slightly longer and thicker. It can therefore be said that this sole modification cannot serve to correct the misbehavior previously described of the $\gamma - Re_{\theta,\mathrm{t}}$ model associated with Spalart and Allmaras' turbulence model. However, the current authors would like to point out that the quantity $\min\{0\ ; S - \Omega\}$ can be kept in mind regarding sensors of laminar separation bubbles turbulence-producing regions.

5.3. Modification of the underlying correlations

This last part presents results obtained with the Spalart-Allmaras model with $\gamma - Re_{\theta,\mathrm{t}}$ transport equations, using the underlying correlations by Langtry and Menter. Figure 13 maps the turbulence shear stress cross-components of these flows. A stronger production of turbulence is achieved with Langtry and Menter's correlations. While not in close agreement with the DNS data, $-\overline{u'v'}/U_\infty^2$ reaches sufficiently higher values for reattachment to occur significantly upstream. The laminar separation bubble is shorter by 10 % and thinner, though the use of these correlations does not prevent the formation of a - smaller than before - secondary separation that is better seen on the friction coefficient evolution represented on figure 14(b). Furthermore, the first rise of turbulence shear stress does not occur significantly earlier with Langtry and Menter's correlations than with Medida and Baeder's, and it is still downstream of the same first rise predicted by DNS. However, relatively to the topology of each flow, this increase in main turbulence shear-stress seems to occur slightly upstream of the summit of the separating line, as in the reference flow. Arguably, the transition displays the proper triggering, but a flawed amplitude : the production of turbulence is much underestimated, yielding the inaccurate topology previously

Figure 13: Reynolds turbulence shear stress cross-components fields obtained with Medida and Baeder's correlations and Langtry and Menter's.

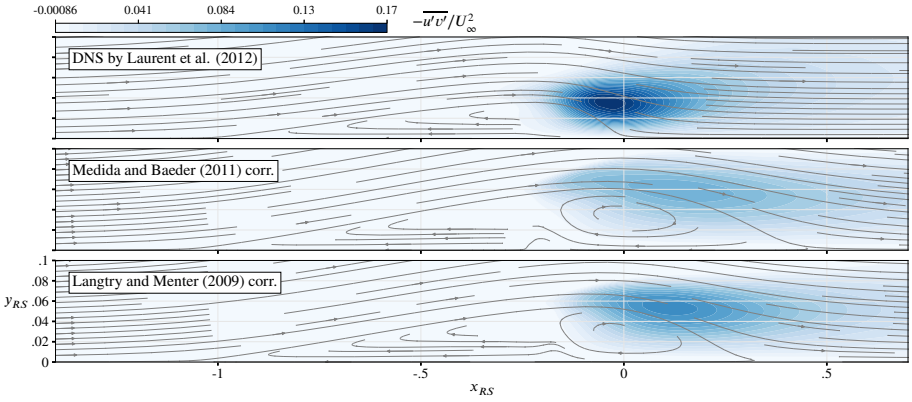

described.

In order to explain the positive influence of the correction, the fields of γ obtained with both versions of the model are represented on figure 15. With the model built on Medida and Baeder's correlations, γ never reaches its asymptotic expected value of 1. On the other hand, changing the correlations allows for a very steep transition, and the transported intermittency variable quickly reaches its target value (upstream of reattachment, in fact). Since γ is used as a pondering factor in the production of $\tilde{\nu}$, the turbulent boundary layer can only be described by the model as intended by Spalart and Allmaras if $\gamma \sim 1$. Using Langtry and Menter's correlations is therefore in better agreement with the original intent of the transition modeling strategy.

The analysis of the boundary-layer caracteristic variables also brings some insight into the effects of modifying the correlations for $Re_{\theta,\mathrm{c}}$ and F_{length}. Figure 14 indicates that the increase in turbulence production allows the turbulent boundary layer to display a better momentum thickness asymptotic slope. Accordingly, the friction coefficient reaches asymptotic values in the fully developed turbulent boundary layer that are closer to those of the reference flow.

Figure 14: Boundary-layer 1-dimensional variables obtained with the $\tilde{\nu} - \gamma - Re_{\theta,\mathrm{t}}$ models completed with two different sets of correlations. (a) : Boundary layer momentum thickness, (b) : Skin friction coefficient.

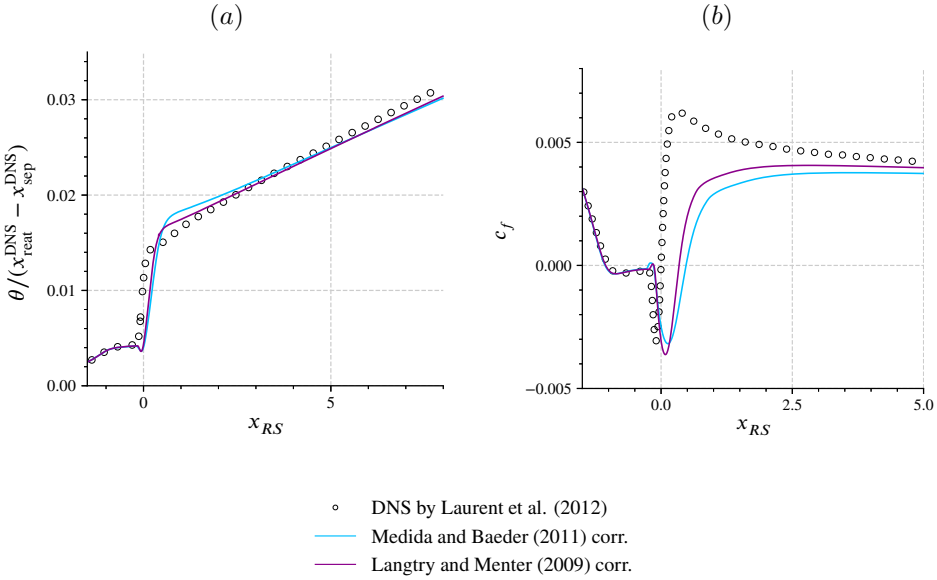

Figure 15: Intermittency fields obtained with Medida and Baeder's correlations and Langtry and Menter's.

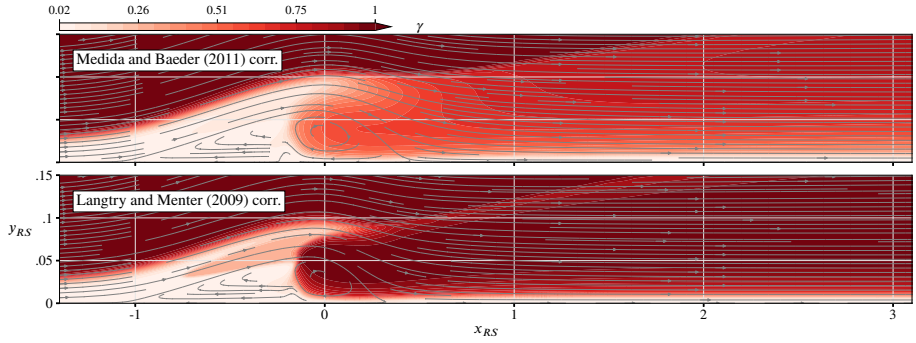

6. Conclusion

In order to assess the performance of the $\gamma - Re_{\theta,\mathrm{t}}$ transition modeling strategy, RANS simulations were run using both turbulence models by Spalart-Allmaras and Menter, coupled to criterion-based and transport equations-based transition models. The chosen test case is a laminar separation bubble on a flat plate designed to mimic that of a leading-edge separation on an airfoil near stall. The reference data comes from a zonal DNS performed by Laurent et al.. In a second part, two modifications were implemented to gain further insight in Medida and Baeder's $\gamma - Re_{\theta,\mathrm{t}}$ transition model. First, the correction by Dacles-Mariani et al. was implemented and used, and the underlying correlations for the variables $Re_{\theta,\mathrm{c}}$ and F_{length} were switched to those by Langtry and Menter [24].

Results were analyzed by comparing flow topologies, turbulence production mechanisms and locations, and boundary layer integral properties. A global tendency of the RANS models towards an underestimation of turbulence production was observed. Therefore, all models build too long a laminar separation bubble, with a good agreement to the reference data regarding the separation point and the start of transition, but a late reattachment, because the pressure recovery is too slow. Furthermore, a second recirculation exists inside the main laminar separation bubble in the flow obtained with the $\tilde{\nu} - \gamma - Re_{\theta,\mathrm{t}}$ model. The authors attribute this flow feature to an internal pressure gradient strong enough for separation, due to the overestimation of the primary separation's size. More problematic is this model's failure to completely switch into its turbulent state downstream of transition, as the transported intermittency γ never reaches its target value of 1. Since this behavior prevents the underlying turbulence model from working as it would in a fully turbulent state for which it has been thoroughly validated, this behavior is regarded as unsound.

Modifying the correlations has yielded significant improvement in the results.

Indeed, the use of Langtry and Menter's correlations instead of Medida and Baeder's allows an increase of γ in the fully turbulent part of the boundary layer, even though they were not originally calibrated for a coupling with this one-equation turbulence model. The predicted transition is steeper and the field of turbulence shear stress cross-components is in better agreement with the reference data, though its peak amplitude is still underestimated by approximately 35 %, and the peak's streamwise location overestimated due to the sluggishness in the production of turbulence. The improvement is noticeable, however, and warrants further research in the design of specifically calibrated correlations.

It was also observed that $k-\omega-$SST-based models display a better behavior in the region near reattachment, where an expected overproduction of turbulence (compared to the asymptotic turbulent boundary layer) should appear, along with a peak of friction coefficient. While this local overproduction of turbulence is the motive of Langtry and Menter's separation correction that makes use of the γ_{sep} and γ_{eff} fields, it appears to be too weak to trigger the Spalart-Allmaras model with a sufficient amplitude. Hence, the friction coefficient distributions obtained with this model display a monotonic behavior downstream of the friction minimum. Recalibrating or reformulating this correction to better account for the overproduction of turbulence is the object of future work.

Finally, the effects of the Dacles-Mariani correction on the flow were not decisive, but the analysis of its activation zones has shown that $\min\{0\ ; S-\Omega\}$ might be an interesting sensor to detect the regions where the turbulence production must increase in laminar separation bubbles. The study could be led further by normalizing this quantity and designing a production-increasing modification to the current $\tilde{\nu}-\gamma-Re_{\theta,\text{t}}$ model.

Along with the previously-mentioned topics, future research will be devoted to extending the $\gamma-Re_{\theta,\text{t}}$ transition modeling framework to the ZDES (mode 2) hybrid RANS-LES method by Deck and Renard (2020) [61].

7. Appendix

7.1. Local correlations-based transition models

Menter et al. (2006) [22] proposed a local correlations-based transition model (LCTM) designed to be coupled to an existing turbulence model. This model is comprised of two transport equations, and a set of correlations to fit the experimental data used for calibration. The first equation (eq. (9)) describes the transport of a first supplemented transported variable, called γ, a numerical intermittency. It is meant to vanish in the laminar regions and to equal 1 in the fully turbulent ones.

$$\mathrm{D}_t\left(\rho\gamma\right) = P_\gamma - D_\gamma + \sum_i \partial_{x_i}\left[\left(\mu + \frac{\mu_\mathrm{t}}{\sigma_\gamma}\right)\partial_{x_i}\gamma\right], \tag{9}$$

The production and destruction terms of this equation are :

$$\begin{cases} P_\gamma = c_{\mathrm{a},1}\rho S F_{\mathrm{length}}\sqrt{F_{\mathrm{onset}}}\left(1 - c_{\mathrm{e},1}\gamma\right)\sqrt{\gamma} \\ D_\gamma = c_{\mathrm{a},2}\rho\Omega\gamma\left(c_{\mathrm{e},2}\gamma - 1\right)F_{\mathrm{turb}} \end{cases} \tag{10}$$

and the underlying functions can be written as :

$$\begin{aligned} F_{\mathrm{onset}} &= \max\left\{F_{\mathrm{onset},2} - F_{\mathrm{onset},3}; 0\right\} \\ F_{\mathrm{onset},3} &= \max\left\{1 - \left(\frac{R_\mathrm{T}}{2.5}\right)^3; 0\right\} \\ F_{\mathrm{onset},2} &= \min\left\{\max\left\{F_{\mathrm{onset},1}; {F_{\mathrm{onset},1}}^4\right\}; 2\right\} \\ F_{\mathrm{onset},1} &= \frac{Re_\mathrm{v}}{2.193\ Re_{\theta,\mathrm{c}}} \\ F_{\mathrm{turb}} &= e^{-\left(\frac{R_\mathrm{T}}{4}\right)^4} \end{aligned} \tag{11}$$

The eddy-to-molecular viscosity ratio $R_\mathrm{T} = \frac{\mu_\mathrm{t}}{\mu}$ is computed from the turbulence variables of the underlying model. As the momentum thickness Reynolds number Re_θ of a boundary layer profile is a non-local property, Menter et al. [22] correlate it to a (local) Reynolds number based either on the local vorticity or on the strain rate in order to build a fully local transition model, as in eq. (12) :

$$Re_\theta = \frac{\max\limits_{y\in[0,\delta]}\left(Re_\mathrm{v}\right)}{2.193}, \text{ where } Re_\mathrm{v} = \frac{y^2}{\nu}S \tag{12}$$

Since this link is only used to describe the position where intermittency needs to start increasing, it is sufficient to detect only the first location where the critical threshold is crossed by the value of Re_{v} (which is therefore its maximum). This observation removes the need for the non-local computation of the maximum function.

The second equation (eq. (13)) describes the dynamics of a second transported variable, $Re_{\theta,\mathrm{t}}$, that propagates boundary layer history downstream.

$$\mathrm{D}_t\left(\rho Re_{\theta,\mathrm{t}}\right) = P_{\theta,\mathrm{t}} + \sum_i \partial_{x_i}\left[\sigma_{\theta,\mathrm{t}}\left(\mu+\mu_{\mathrm{t}}\right)\partial_{x_i} Re_{\theta,\mathrm{t}}\right] \tag{13}$$

The production term of this equation is :

$$P_{\theta,\mathrm{t}} = c_{\theta,\mathrm{t}}\frac{\rho}{\tau}\left(Re_{\theta,\mathrm{S}} - Re_{\theta,\mathrm{t}}\right)\left(1-F_{\theta,\mathrm{t}}\right), \tag{14}$$

where t is a time scale :

$$\tau = \frac{500\nu}{U^2} \tag{15}$$

and $Re_{\theta,\mathrm{S}}$ is the value of the momentum thickness-based Reynolds number at the start of transition as the intermittency first starts to increase in the boundary layer. This value is determined by a correlation.

The production activation function reads :

$$F_{\theta,\mathrm{t}} = \max\left\{e^{-\left(\frac{y}{\delta}\right)^4}; 1-\left(\frac{c_{\mathrm{e},2}\gamma-1}{c_{\mathrm{e},2}-1}\right)^2\right\} \tag{16a}$$

where :

$$\delta = \frac{50\ \Omega y}{U}\delta_{\mathrm{BL}}\ ;\ \delta_{\mathrm{BL}} = \frac{15}{2}\theta_{\mathrm{BL}} \text{ and } \theta_{\mathrm{BL}} = \frac{Re_{\theta,\mathrm{t}}\nu}{U} \tag{16b}$$

Note that Menter et al. used a function named F_{wake} to prevent the model from behaving the same way in a free shear layer as in a boundary layer. Since the computation of this function involves the local value of the specific dissipation rate of turbulent kinetic energy, ω, it is omitted when the underlying turbulence model is that of Spalart and Allmaras [40].

Table 6: Calibration constants of the $\gamma - Re_{\theta,\mathrm{t}}$ model [24].

Constant name	$c_{\mathrm{e},1}$	$c_{\mathrm{e},2}$	$c_{\mathrm{a},1}$	$c_{\mathrm{a},2}$	σ_γ	$c_{\theta,\mathrm{t}}$	$\sigma_{\theta,\mathrm{t}}$
Value	1	50	2	0.06	1	0.03	2

Acknowledgements

The authors would like to deeply thank Luis Bernardos for his help with physical aspects of transition, its modeling and, more practically, his ideas and scripts for presenting data. Many thanks also to Vincent Gleize for useful exchanges regarding the workings of the (numerous) terms of the $\gamma - Re_{\theta,\mathrm{t}}$ framework. Finally, let the funding effort by *Délégation Générale pour l'Armement - Centre Essais Propulseurs* be acknowledged.

References

[1] D. E. Halstead, D. C. Wisler, T. H. Okiishi, G. J. Walker, H. P. Hodson, H.-W. Shin, Boundary layer development in axial compressors and turbines: Part 2 of 4 — compressors, in: Turbo Expo: Power for Land, Sea, and Air, Vol. Volume 1: Turbomachinery, 1995, pp. 1–20, v001T01A110. doi:10.1115/95-GT-462.

[2] D. E. Halstead, D. C. Wisler, T. H. Okiishi, G. J. Walker, H. P. Hodson, H.-W. Shin, Boundary layer development in axial compressors and turbines: Part 3 of 4 — LP turbines, in: Turbo Expo: Power for Land, Sea, and Air, Vol. Volume 1: Turbomachinery, 1995, pp. 1–15, v001T01A111. doi:10.1115/95-GT-463.

[3] F. Richez, A. Le Pape, M. Costes, Zonal Detached-Eddy Simulation of separated flow around a finite-span wing, AIAA Journal 53 (11) (2015) 3157 – 3166. doi:10.2514/1.J053636.

[4] A. Hatman, T. Wang, Separated flow transition - part 2 : Experimental results, in: ASME Turbo Expo: Power for Land, Sea, and Air, 1998, pp. 1–12. doi:10.1115/98-GT-462.

[5] R. J. Volino, L. S. Hultgren, Measurements in separated and transitional boundary layers under low-pressure turbine airfoil conditions, Journal of Turbomachinery 123 (2) (2000) 189 – 197. doi:10.1115/1.1350408.

[6] S. K. Roberts, M. I. Yaras, Measurements and prediction of free-stream turbulence and pressure-gradient effects on attached-flow boundary-layer transition, in: Turbo Expo: Power for Land, Sea, and Air, Vol. Volume 5: Turbo Expo 2003, Parts A and B, 2003, pp. 729–743. doi:10.1115/GT2003-38261.

[7] A. Hatman, T. Wang, Separated flow transition - part 1 : Experimental methodology and mode classification, in: ASME Turbo Expo: Power for Land, Sea, and Air, 1998, pp. 1–10. doi:10.1115/98-GT-461.

[8] M. Alam, N. D. Sandham, Direct numerical simulation of 'short' laminar separation bubbles with turbulent reattachment, Journal of Fluid Mechanics 410 (2000) 1–28. doi:10.1017/S0022112099008976.

[9] S. K. Roberts, M. I. Yaras, Large-Eddy Simulation of transition in a separation bubble, Journal of Fluids Engineering 128 (2) (2005) 232–238. doi:10.1115/1.2170123.

[10] B. R. McAuliffe, M. I. Yaras, Numerical study of instability mechanisms leading to transition in separation bubbles, Journal of Turbomachinery 130 (2008) 021006. doi:10.1115/1.2750680.

[11] R. J. Volino, Separated flow measurements on a highly loaded low-pressure turbine airfoil, Journal of Turbomachinery 132. doi:10.1115/1.3104608.

[12] P. R. Owen, L. Klanfer, On the laminar boundary layer separation from the leading edge of a thin aerofoil, Tech. rep., Aeronautical Research Council, report n. Aero2508 (Oct. 1953).

[13] E. Dick, S. Kubacki, Transition models for turbomachinery boundary layer flows: a review, International Journal of Turbomachinery, Propulsion and Power 2 (2) (2017) 4.

[14] H. W. Emmons, The laminar-turbulent transition in the boundary layer - part I, Journal of Aerospace Science 18 (1951) 490–498.

[15] S. Dhawan, R. Narasimha, Some properties of boundary layer flow during the transition from laminar to turbulent motion, Journal of Fluid Mechanics 3 (4) (1958) 418–436. doi:10.1017/S0022112058000094.

[16] W. B. Roberts, Calculation of laminar separation bubbles and their effect on airfoil performance, AIAA journal 18 (1) (1980) 25–31. doi:10.2514/3.50726.

[17] A. Hatman, T. Wang, A prediction model for separated-flow transition, in: ASME Turbo Expo: Power for Land, Sea, and Air, 1998, pp. 1–10. doi:10.1115/98-GT-237.

[18] N. J. Seyb, A simplified and practical method of determining the external heat-transfer coefficient round a turbine blade, Tech. Rep. 29398, ARC (Sep. 1967).

[19] B. J. Abu-Ghannam, R. Shaw, Natural transition of boundary layers. The effect of turbulence, pressure gradient, and flow history, Journal of Mechanical Engineering Science 22 (5) (1980) 213–228. doi:10.1243/JMES_JOUR_1980_022_043_02.

[20] R. E. Mayle, The role of laminar-turbulent transition in gas turbine engines, Journal of Turbomachinery 113 (4) (1991) 509–536. doi:10.1115/1.2929110.

[21] L. Bernardos, F. Richez, V. Gleize, G. A. Gerolymos, Algebraic nonlocal transition modeling of laminar separation bubbles using $k - \omega$ turbulence models, AIAA Journal 57 (2) (2019) 553–565. doi:10.2514/1.J057734.

[22] F. R. Menter, R. B. Langtry, S. R. Likki, Y. B. Suzen, P. G. Huang, S. Völker, A correlation-based transition model using local variables - part I : Model formulation, Journal of Turbomachinery 128 (2006) 413–422. doi:10.1115/1.2184352.

[23] J. G. Coder, Enhancement of the Amplification Factor Transport transition modeling framework, in: 55th AIAA Aerospace Sciences Meeting, 2017, p. 1709. doi:10.2514/6.2017-1709.

[24] R. B. Langtry, F. R. Menter, Correlation-based transition modeling for unstructured parallelized computational fluid dynamics codes, AIAA Journal 47 (12) (2009) 2894–2906. doi:10.2514/1.42362.

[25] R. B. Langtry, K. Sengupta, D. T. Yeh, A. J. Dorgan, Extending the $\gamma - \overline{Re_{\theta,t}}$ local correlation-based transition model for crossflow effectsdoi:10.2514/6.2015-2474.

[26] C. M. Langel, R. Chow, C. P. Van Dam, M. A. Rumsey, D. C. Maniaci, R. S. Ehrmann, E. B. White, A computational approach to simulating the effects of realistic surface roughness on boundary layer transition. doi:10.2514/6.2014-0234.

[27] C. Son, M. Kelly, T. Kim, Boundary-layer transition model for icing simulations of rotating wind turbine blades, Renewable Energy 167 (2021) 172–183. doi:j.renene.2020.11.070.

[28] C. Ye, F. Wang, C. Wang, B. P. M. van Esch, Assessment of turbulence models for the boundary layer transition flow simulation around a hydrofoil, Ocean Engineering 217 (2020) 108124. doi:10.1016/j.oceaneng.2020.108124.

[29] K. Liu, Y. Wang, W.-P. Song, Z.-H. Han, A two-equation local-correlation-based laminar-turbulent transition modeling scheme for external aerodynamics, Aerospace Science and Technology 106 (2020) 106128. doi:10.1016/j.ast.2020.106128.

[30] C. Sheng, Improving predictions of transitional and separated flows using RANS modeling, Aerospace Science and Technology (2020) 106067doi:10.1016/j.ast.2020.106067.

[31] P. R. Spalart, S. R. Allmaras, A one-equation turbulence model for aerodynamic flows, in: 30th Aerospace Sciences Meeting and Exhibit, Vol. 94, American Institute of Aeronautics and Astronautics, Reno, NV, U.S.A., 1992, pp. 1–22. doi:10.2514/6.1992-439.

[32] F. R. Menter, Two-equation eddy-viscosity turbulence models for engineering applications, AIAA Journal 32 (8) (1994) 1598–1605. doi:10.2514/3.12149.

[33] C. Laurent, I. Mary, V. Gleize, A. Lerat, D. Arnal, DNS database of a transitional separation bubble on a flat plate and application to RANS modeling validation, Computers & Fluids 61 (0) (2012) 21 – 30, high Fidelity Flow Simulations, Onera Scientific Day. doi:10.1016/j.compfluid.2011.07.011.

[34] D. Arnal, M. Habiballah, E. Coustols, Théorie de l'instabilité laminaire et critères de transition en écoulement bi- et tridimensionnel, La Recherche Aérospatiale 2 (1984) 125–143.

[35] M. T. Arthur, H. S. Dol, A. Krumbein, R. Houdeville, J. Ponsin, Application of transition criteria in Navier-Stokes computations, Tech. rep., GARTEUR/TP-137 (Jan. 2003).

[36] C. Gleyzes, J. Cousteix, J. Bonnet, Theoretical and experimental study of low Reynolds number transitional separation bubbles, in: UNDAS-CP-77B123, Conference on low Reynolds number airfoil aerodynamics, 1985.

[37] Y. B. Suzen, G. Xiong, P. G. Huang, Predictions of transitional flows in low-pressure turbines using intermittency transport equation, AIAA Journal 40 (2) (2002) 254–266. doi:10.2514/2.1667.

[38] P. Catalano, B. Mele, R. Tognaccini, On the implementation of a turbulence model for low Reynolds number flows, Computers & Fluids 109 (2015) 67–71. doi:10.1016/j.compfluid.2014.12.009.

[39] L. Bernardos, F. Richez, V. Gleize, RANS modeling of laminar separation bubbles around airfoils at low Reynolds conditions, 2019. doi:10.2514/6.2019-2922.

[40] S. Medida, J. D. Baeder, Application of the correlation-based $\gamma - \tilde{Re}_{\theta t}$ transition model to the Spalart-Allmaras turbulence model, in: 20th AIAA Computational Fluid Dynamics Conference, Honolulu, Hawaii, American Institute of Aeronautics and Astronautics, 2011, pp. 1–21. doi:10.2514/6.2011-3979.

[41] J. Dacles-Mariani, G. Zilliac, J. Chow, P. Bradshaw, Numerical/experimental study of a wingtip vortex in the near field, AIAA Journal 33 (1995) 1561–1568. doi:10.2514/3.12826.

[42] S. K. Roberts, M. I. Yaras, Modeling transition in separated and attached boundary layers, Journal of Turbomachinery 127 (2) (2004) 402–411. doi:10.1115/1.1860570.

[43] J. Dunham, Prediction of boundary layer transition on turbomachinery blades, in: AGARD AG-64(3) Meeting Boundary Layer in Turbomachines, 1972.

[44] D. J. Hall, J. C. Gibbings, Influence of stream turbulence and pressure gradient upon boundary layer transition, Journal of Mechanical Engineering Science 14 (2) (1972) 134–146. doi:10.1243/JMES_JOUR_1972_014_019_02.

[45] J. Hourmouziadis, Aerodynamic design of low pressure turbines, in: Blading Design for Axial Turbomachines, AGARD Lecture series, 1989, pp. 8–40.

[46] R. B. Langtry, A correlation-based transition model using local variables for unstructured parallelized CFD codes, Ph.D. thesis, Institut für Thermische Strömungsmaschinen und Maschinenlaboratorium, Universität Stuttgart (2006).

[47] M. Krause, M. Behr, J. Ballmann, Modeling of transition effects in hypersonic intake flows using a correlation-based intermittency model, in: 15th AIAA International Space Planes and Hypersonic Systems and Technologies Conference, American Institute of Aeronautics and Astronautics, 2008, pp. 1–12. doi:10.2514/6.2008-2598.

[48] K. Suluksna, P. Dechaumphai, E. Juntasaro, Correlations for modeling transitional boundary layers under influences of freestream turbulence and pressure gradient, International Journal of Heat and Fluid Flow 30 (1) (2009) 66–75. doi:10.1016/j.ijheatfluidflow.2008.09.004.

[49] C. Content, R. Houdeville, Local correlation-based transition model, in: 8th International ERCOFTAC Symposium on Engineering Turbulence Modelling and Measurements, 2010, pp. 522–527.

[50] C. Content, Méthode innovante pour le calcul de la transition laminaire-turbulent dans les codes Navier-Stokes, Ph.D. thesis, Institut Supérieur de l'Aéronautique et de l'Espace, Université de Toulouse, France (2011).

[51] A. Minot, X. de Saint Victor, J. Marty, J. Perraud, Advanced numerical setup for separation-induced transition on high-lift low-pressure turbine flows using the $\gamma-\widetilde{R_{\theta_t}}$ model, in: ASME Turbo Expo 2015: Turbine Technical Conference and Exposition, American Society of Mechanical Engineers, 2015, pp. V02BT39A010–V02BT39A010. doi:10.1115/GT2015-42160.

[52] A. Minot, Modélisation de la transition laminaire-turbulent par rugosité et bulbe de décollement laminaire sur les aubes de turbomachines, Thèses, Université de Toulouse, Institut Supérieur de l'Aéronautique et de l'Espace (ISAE-Supaéro) (May 2016).

[53] B. R. Smith, A near wall model for the $k-l$ two equation turbulence model, in: AIAA, Fluid Dynamics Conference, 25 th, Colorado Springs, CO, 1994.

[54] L. Cambier, S. Heib, S. Plot, The Onera elsA CFD software: input from

research and feedback from industry, Mechanics & Industry 14 (2013) 159–174. doi:10.1051/meca/2013056.

[55] A. Le Pape, M. Costes, F. Richez, G. Joubert, F. David, J.-M. Deluc, Dynamic stall control using deployable leading-edge vortex generators, AIAA Journal 50 (10) (2012) 2135–2145. doi:10.2514/1.J051452.

[56] R. J. Shyne, K.-H. Sohn, K. J. De Witt, Experimental investigation of boundary layer behavior in a simulated low pressure turbine, Journal of Fluids Engineering 122 (1) (1999) 84–89. doi:10.1115/1.483229.

[57] W. Lou, J. Hourmouziadis, Separation bubbles under steady and periodic-unsteady main flow conditions, Journal of Turbomachinery 122 (4) (2000) 634–643. doi:10.1115/1.1308568.

[58] C. Laurent, Study of transitional and non-equilibrium flows through DNS and RANS approaches., Theses, Ecole nationale supérieure d'arts et métiers - ENSAM (Dec. 2012).

[59] Z. Hall, Assessment of transition modeling capabilities in nasa's overflow cfd code version 2.2m, in: 2018 AIAA Aerospace Sciences Meeting, 2018. doi:10.2514/6.2018-0032.

[60] M.-S. Liou, A sequel to AUSM, part II: AUSM+-up for all speeds, Journal of Computational Physics 214 (1) (2006) 137 – 170. doi:10.1016/j.jcp.2005.09.020.

[61] S. Deck, N. Renard, Towards an enhanced protection of attached boundary layers in hybrid RANS/LES methods, Journal of Computational Physics (2020) 108970doi:10.1016/j.jcp.2019.108970.